

Arithmetic Distribution Neural Network for Background Subtraction

Chenqiu Zhao, *Student Member, IEEE* Kangkang Hu and Anup Basu, *Senior Member, IEEE*

Abstract—We propose a new Arithmetic Distribution Neural Network (ADNN) for learning the distributions of temporal pixels during background subtraction. In our ADNN, the arithmetic distribution operations are utilized to propose the arithmetic distribution layers, including the product distribution layer and the sum distribution layer. Furthermore, in order to improve the accuracy of the proposed approach, an improved Bayesian refinement model based on neighboring information, with a GPU implementation, is introduced. In the forward pass and backpropagation of the proposed arithmetic distribution layers, histograms are considered as probability density functions rather than matrices. Thus, the proposed approach is able to utilize the probability information of the histogram and achieve promising results with a very simple architecture compared to traditional convolutional neural networks. Evaluations using standard benchmarks demonstrate the superiority of the proposed approach compared to state-of-the-art traditional and deep learning methods. To the best of our knowledge, this is the first method to propose network layers based on arithmetic distribution operations for learning distributions during background subtraction.

Index Terms—Background Subtraction, Deep Learning, Distribution Learning, Arithmetic Distribution Operations

I. INTRODUCTION

Background subtraction is a fundamental research topic related to motion detection in computer vision, which has attracted increasing attention during a period of explosive growth in video streaming. Traditionally, background subtraction algorithms are closely related to distribution analysis, since the distribution of temporal pixels plays an important role in identifying a pixel as foreground or background. Sophisticated models including deep learning networks have been devised for distribution analysis in background subtraction. Unfortunately, when a convolutional neural network is involved, the histograms, which describe distributions, are considered as feature vectors rather than a probability density function. This is an arbitrary utilization of matrix arithmetic operations since the probability information is ignored, limiting the ability of algorithms based on convolutional neural networks for analyzing complex distributions. Thus, distribution analysis based on convolutional neural networks remains a challenging problem.

In background subtraction, pixels are classified as foreground or background based on comparisons with their historical counterparts. Thus, the distribution of comparisons is a useful feature that can be directly input into the network

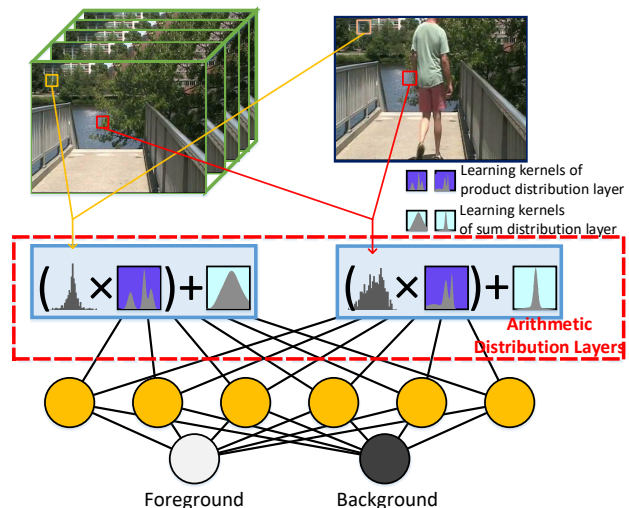


Fig. 1. Illustration of the arithmetic distribution neural network for background subtraction. Histograms of subtractions between the current observations and their historical counterparts in pixels are input into the arithmetic distribution layers, containing the product and sum distribution layers for distribution learning. In particular, the learning kernels of arithmetic distributions layers are also distributions. A classification architecture is then attached to label the pixels according to the output of these layers.

for classification. However, when distributions are converted into histograms for the convolution operation, they are actually considered as feature vectors in which the probabilistic information is ignored. However, the essence of a histogram is the probability density function which describes the distributions of random variables. In this work, the arithmetic distribution operations [1], which are used to compute the distribution of arithmetic operations of random variables having known distributions, are derived to serve as an alternative to matrix arithmetic operations. This enables histograms to be considered as probability density functions rather than feature vectors. Based on the new operations, we propose the arithmetic distribution layers containing the product and the sum distribution layers for learning and classifying distributions. Thereby, a novel Arithmetic Distribution Neural Network (ADNN) including arithmetic distribution layers is devised for background subtraction, as shown in Fig. 1.

The architecture of the proposed ADNN is quite straightforward. Histograms of subtractions between pixels' current observations and their historical counterparts are used as the input to the arithmetic distribution layers containing the product distribution layer and the sum distribution layer. Specifi-

The authors are with the Dept. of Computing Science and UAHJIC, University of Alberta, Edmonton, AB T6G 2E1, Canada (Contact e-mails: zhaochenqiu@gmail.com, zhao.chenqiu@ualberta.ca, hukang_cmu@126.com. and basu@ualberta.ca)

cally, the learning kernels are also histograms and considered as probability density functions. Both the forward pass and backpropagation of layers are based on arithmetic distribution operations. A classification architecture is attached to label pixels according to the output of the arithmetic distribution layers. In particular, the classification architecture is kept as simple as possible, with only one convolutional layer, one rectified linear unit layer, and one fully connected layer, to demonstrate that the good performance of the proposed approach comes from the proposed arithmetic distribution layers. Unfortunately, since pixels are classified independently, the proposed approach is sensitive to noisy points that can be handled by neighboring information. An improved Bayesian refinement model, with a GPU implementation, is thus proposed for noise compensation. By utilizing the arithmetic distribution operations, histograms can be considered as probability density functions, with the probability information being utilized. This helps the proposed approach achieve promising results compared to even convolutional neural networks. Furthermore, since the histograms of temporal pixels are pixelwise features, a large number of training instances can be captured. Thus, the proposed approach requires fewer than 1% of the ground truth frames during training. In addition, since the distribution information of temporal pixels is independent of scene information, the proposed network does not rely too much on the scenes where training frames are captured. Our ADNN can be trained with video frames obtained from different scenes, and it is valid even when no frame from the scenes of the testing videos is included in the training set.

The main contributions of this paper are:

- We propose the Arithmetic Distribution Neural Network (ADNN) for background subtraction, utilizing the product distribution layer and the sum distribution layer.
- An improved Bayesian refinement model, with a GPU implementation, is proposed to improve the accuracy of the proposed approach. In particular, an approximation of the Gaussian function is utilized to compute the correlation between neighboring pixels.
- Comprehensive experiments are conducted to evaluate the proposed approach, including: a) validating the correctness of the proposed product distribution layer and the sum distribution layer, as shown in Section V-A; b) comparisons between the proposed ADNN and traditional convolutional neural networks on real data are shown in Section V-B; c) a discussion on the generality of the proposed approach under the condition that training frames and testing frames are randomly captured from different scenes, as shown in Section V-C; and, d) a comprehensive comparison between the proposed approach and state-of-the-art methods including traditional and deep learning approaches on standard benchmarks, as shown in Section V-D.

II. RELATED WORK

In this section, we outline background subtraction algorithms briefly into three categories. In Section II-A, traditional background subtraction algorithms are introduced.

Background subtraction based on deep learning network is discussed in Section II-B. Finally, distribution learning techniques and their relation to background subtraction methods are described in Section II-C.

A. Traditional Algorithms

Traditional algorithms [2]–[29] have focused on capturing background representation from temporal pixels for subtraction, usually based on artificial models. In particular, the Gaussian mixture model is one of the most popular techniques [21], where the background observations are described by several Gaussian functions [4], [22], with a large number of extensions being proposed [19], [20]. In addition, several excellent publications [17], [24]–[26] have considered the background as an low-rank component of video frames, given the correlation between background scenes of frames over time. For example, Javed et al. [25], [26] utilized robust principal component analysis [24] to separate the background scenes based on the spatial and temporal subspaces. Yong et al. [17] proposed online matrix factorization for background subtraction. Machine-learning techniques have also been utilized for background subtraction [30]–[40]. Lin et al. [30] classified the pixels by using a probabilistic support vector machine. Similarly, Han et al. [32] used the density-based features into a classifier based on a support vector machine for classification. Li et al. [31] formulated background subtraction as minimizing a constrained risk function and Culibrk et al. [35] proposed an unsupervised Bayesian classifier using a neural network architecture for background subtraction. Unfortunately, given the complexity and diversity of natural scenes, artificial models are not adequate to generate a perfect classification of pixels for background subtraction. In this work, we propose the arithmetic distribution neural network to automatically learn the distributions of pixels for background subtraction.

B. Algorithms based on Deep Learning

Recently, several excellent approaches [15], [41]–[57] have used deep learning networks to learn the background scenes for subtraction. For example, Wang et al. [47] proposed a fully connected network to learn the background scenes, and Zeng et al. [50] utilized a multi-scale strategy to improve the results. Similarly, Lim et al. [48] used a triplet convolutional neural network to extract multi-scale features from background scenes, and Yang et al. [41] improved the robustness of their method by using an end-to-end multi-scale spatio-temporal (MS-ST) method to extract deep features from scenes. Unfortunately, these papers usually assumed a large number of ground truth frames for training, which is very expensive in background subtraction applications. Also, these approaches rely considerably on the scene information, which limits them to the condition that the testing frames and training frames must be captured from the same video. In contrast, Mandal et al. [42], [43] proposed a spatio-temporal feature learning network for background subtraction in unseen videos, but a large number of annotated frames are still assumed during training. In addition, Babaei et al. [52] proposed a robust model in which a network is used to subtract the background

from the current frame and only 5% of the labeled masks are utilized for training. Liang et al. [53] utilized the foreground mask generated by the SubSENSE algorithm [15] rather than manual labeling for training, and Zeng et al. [54] used a convolutional neural network to combine several background subtraction algorithms together. In our work, since the distributions of temporal pixels are captured from every spatial pixel, a large number of training instances can be captured with a limited number of ground truth frames. Thus, our proposed approach requires less than 1% of the ground truth frames for training. Because the distribution information is independent of the scene information, our proposed ADNN is effective even when the training videos and testing videos are completely different.

C. Distribution Learning and Background Subtraction

The distribution of temporal pixels plays an important role [3], [4], [7], [8], [58]–[70] throughout the development of background subtraction algorithms, since it is a good representation of background information. In particular, the Gaussian mixture model proposed by Zivkovic et al. [4] is one of the most popular techniques as we mentioned above. In addition, Lee et al. [3] utilized an adaptive learning rate for each Gaussian function to improve the convergence rate during clustering, and Haines et al. [8] [58] used the Dirichlet processes with Gaussian mixture models to analyze pixel distributions. Recently, Chen et al. [59] [60] used Gaussian mixture models to represent the vertices of spanning trees and Akilan et al. [61] proposed a foreground validation process through probability estimation of multivariate Gaussian model distribution. Besides the Gaussian distribution, there are also several other techniques for the description of temporal pixels, such as Laplacian distribution [62], kernel density estimation [63] and artificial neural networks [64].

Unfortunately, artificial models do not have the ability to handle the complex distributions generated from diverse natural scenes. Thus, learning-based algorithms [71], such as convolutional neural networks, attract our attention. However, most existing distribution learning algorithms are related to label distribution learning [71]–[76]. They handle insufficient training data based on label ambiguity, rather than classifying two distributions. Instead, Zhao et al. [77], [78] proposed deep pixel distribution learning in which the temporal pixels are randomly permuted to force the network to focus on the statistical distribution information. It is actually a simulation procedure to capture the expected value of the distribution of products of entries in the input patch and the learning kernel. However, the random permutation process is time-consuming since a number of random numbers need to be generated. Besides, there are many useful features of distributions are dropped since the output of a layer is the expected value. In contrast, in this work we propose the arithmetic distribution layers to compute the distribution of products of random variables having distributions implied in the input and learning kernel. The output of the layer is the entire distribution described by a histogram rather than an expected value, which contributes to better performance of the proposed approach,

since more information is utilized for distribution analysis. A comprehensive comparison between the proposed approach and Zhao et al.’s work is given in Section V-D.

III. ARITHMETIC DISTRIBUTION LAYERS

To the best of our knowledge, distributions have to be converted to histograms for convolutions in which the matrix arithmetic operations are used; and, all the objects involved in the operations are considered as vectors. In this condition, the correlation between the entries of a histogram as well as their probability information are ignored. Essentially, histograms are probability density functions that describe the distributions of random variables. When a histogram of a distribution is input into a network for classification, it is actually the random variable that has the input distribution that needs classification. Therefore, a network layer based on the arithmetic of random variables having distributions of the input and the learning kernel is supposed to be a more reasonable substitute for the convolution layer. In addition, the arithmetic distribution operations, which refer to the operations that compute the distribution of arithmetic results of random variables having known distributions, are derived to serve as a better substitute of the matrix arithmetic operations. In this work, the arithmetic distribution layers including the product and sum distribution layers based on arithmetic distribution operations are proposed. In particular, both the input and the learning kernels of layers are considered as probability density functions, which are described by histograms; and, arithmetic distribution operations are used in the forward pass and backpropagation for learning a distribution.

The product distribution layer is used to compute the distribution of the product of random variables having distributions described by the histograms of the input and learning kernel. Assume two independent, continuous random variables X and W , which are described by probability density functions $f_X(x)$ and $f_W(w)$ respectively. Both $f_X(x)$ and $f_W(w)$ are represented by histograms. In particular, $f_X(x)$ is assumed to be the input histogram of the product distribution layer, and $f_W(w)$ denotes the histogram of the learning kernel. The output of the product distribution layer $f_Z(z)$ is actually the probability density function of the random variable $Z = XW$, which is the product of X and W . In order to capture the expression for $f_Z(z)$, the definition of the cumulative distribution function of Z is proposed first, as shown below:

$$\begin{aligned} F_Z(z) &\stackrel{def}{=} \mathbb{P}(Z \leq z) = \mathbb{P}(XW \leq z) \\ &= \mathbb{P}(XW \leq z, W \geq 0^+) + \mathbb{P}(XW \leq z, W \leq 0^-) \quad (1) \\ &= \mathbb{P}(X \leq \frac{z}{W}, W \geq 0^+) + \mathbb{P}(X \geq \frac{z}{W}, W \leq 0^-), \end{aligned}$$

where $F_Z(z)$ is the cumulative distribution function of the random variable Z . \mathbb{P} is a cumulative distribution under a particular condition. Next, assuming X , W and Z are between negative infinity and positive infinity, the expression of $F_Z(z)$ is converted into an expression following the cumulative

distribution function. Mathematically, this can be shown as:

$$\begin{aligned}
F_Z(z) &= \int_0^\infty f_W(w) \int_{-\infty}^{\frac{z}{w}} f_X(x) dx dw + \int_{-\infty}^0 f_W(w) \int_{\frac{z}{w}}^\infty f_X(x) dx dw \\
\therefore \mathbb{P}(X \leq \frac{z}{W}, W \geq 0^+) &= \int_0^\infty f_W(w) \int_{-\infty}^{\frac{z}{w}} f_X(x) dx dw \\
\mathbb{P}(X \geq \frac{z}{W}, W \leq 0^-) &= \int_{-\infty}^0 f_W(w) \int_{\frac{z}{w}}^\infty f_X(x) dx dw,
\end{aligned} \tag{2}$$

where dx and dw are the delta of x and w respectively. Finally, with the help of the Leibniz integral rule, the probability density function $f_Z(z)$ of Z can be obtained as the derivative of the cumulative distribution function $F_Z(z)$. This is expressed as:

$$\begin{aligned}
f_Z(z) &= \frac{d(F_Z(z))}{dz} \\
&= d\left(\int_0^\infty f_W(w) \int_{-\infty}^{\frac{z}{w}} f_X(x) dx dw + \int_{-\infty}^0 f_W(w) \int_{\frac{z}{w}}^\infty f_X(x) dx dw\right) / dz \\
&= \int_{0^+}^\infty f_W(w) f_X\left(\frac{z}{w}\right) \frac{1}{w} dw - \int_{-\infty}^{0^-} f_W(w) f_X\left(\frac{z}{w}\right) \frac{1}{w} dw \\
&= \int_{-\infty}^\infty f_W(w) f_X\left(\frac{z}{w}\right) \frac{1}{|w|} dw \\
\Rightarrow z_j &= \sum_{i=-\infty}^\infty w_i f_X\left(\frac{z_j}{i}\right) \frac{1}{|i|} \cdot 1 \quad \because dw = 1, f_W(i) = w_i,
\end{aligned} \tag{3}$$

where w_i and z_j are the entries of histograms that are used to describe the probability density functions $f_W(w)$ and $f_Z(z)$ corresponding to random variables W and Z , respectively. i and j are the indices of the entries. The formula for the forward pass of the product distribution layer is thus derived. Then, the gradient of $f_W(w)$, which is used to update w_i during backpropagation, is obtained by partial derivatives and the chain rule. Mathematically:

$$\begin{aligned}
\frac{\partial loss}{\partial w_i} &= \frac{\partial loss}{\partial Z} \cdot \frac{\partial Z}{\partial w_i} = \sum_{j=-\infty}^\infty \frac{\partial loss}{\partial z_j} \cdot \frac{\partial z_j}{\partial w_i} \\
&= \sum_{j=-\infty}^\infty \frac{\partial loss}{\partial z_j} \cdot \frac{\partial \left(\sum_{i=-\infty}^\infty w_i f_X\left(\frac{z_j}{i}\right) \frac{1}{|i|} \right)}{\partial w_i} \\
&= \sum_{j=-\infty}^\infty \delta z_j f_X\left(\frac{z_j}{i}\right) \frac{1}{|i|} \\
\Rightarrow \delta w_i &= \sum_{j=-\infty}^\infty \delta z_j f_X\left(\frac{z_j}{i}\right) \frac{1}{|i|}, \\
\text{notation : } \delta S &\equiv \frac{\partial loss}{\partial S}
\end{aligned} \tag{4}$$

where δw_i and δz_j are the gradients of entries of histograms which are utilized to update $f_W(w)$ and $f_Z(z)$ respectively, i and j are indices of entries of histograms, $loss$ is the output of the product distribution layer which is used to compare with the target output to compute the gradient $\partial loss$. This

way, the formula for backpropagation of the proposed product distribution layer is derived.

Similarly, the sum distribution layer is used to compute the distribution of the sum of two random variables X and B , which are described by $f_X(x)$ and $f_B(b)$ respectively. Similar to the product distribution layer, $f_X(x)$ and $f_B(b)$ are represented by histograms as well. Utilizing the same mathematical procedure as the product distribution layer, the expression of the probability density function of the sum $Z = X + B$ of X and B is obtained. Mathematically:

$$\begin{aligned}
f_Z(z) &= \int_{-\infty}^\infty f_B(b) f_X(z-b) db \\
\Rightarrow z_j &= \sum_{i=-\infty}^\infty b_i f_X(z_j - i) \cdot 1 \quad \because db = 1, f_B(i) = b_i,
\end{aligned} \tag{5}$$

where b_i and z_j are the entries of histograms utilized to describe $f_B(b)$ and $f_Z(z)$ corresponding to random variables B and Z , respectively. i and j are indices. Also, the formula for backpropagation is:

$$\begin{aligned}
\frac{\partial loss}{\partial b_k} &= \frac{\partial loss}{\partial Z} \cdot \frac{\partial Z}{\partial b_k} = \sum_{j=-\infty}^\infty \frac{\partial loss}{\partial z_j} \cdot \frac{\partial z_j}{\partial b_k} \\
&= \sum_{j=-\infty}^\infty \frac{\partial loss}{\partial z_j} \cdot \frac{\partial \left(\sum_{i=-\infty}^\infty b_i f_X(z_j - i) \right)}{\partial b_k} \\
&= \sum_{j=-\infty}^\infty \frac{\partial loss}{\partial z_j} \cdot f_X(z_j - k) \\
\Rightarrow \delta b_k &= \sum_{j=-\infty}^\infty \delta z_j f_X(z_j - k), \\
\text{notation : } \delta S &\equiv \frac{\partial loss}{\partial S}
\end{aligned} \tag{6}$$

where δb_k and δz_j are the gradients of entries in histograms corresponding to $f_B(b)$ and $f_Z(z)$ respectively, and k and j are indices. $loss$ is the output of the sum distribution layer which is used to compare with the target output to compute the gradient for updating the sum distribution layer.

With the help of Eqn. 3–6, the forward pass and the backpropagation of arithmetic distribution layers can be easily implemented by Pytorch [79]. In particular, the gradient of learning kernels of arithmetic distribution layers is computed and input into the ‘‘Autograd package’’ of PyTorch [79] for backpropagation. Moreover, a validation experiment based on synthetic data is proposed in Section V-A to verify the correctness of the proposed product and sum distribution layers. In the experiments, the arithmetic distribution layers are fed with data from a few synthetic distributions, in order to validate their ability of distribution learning.

IV. ARITHMETIC DISTRIBUTION NEURAL NETWORK FOR BACKGROUND SUBTRACTION

Utilizing the proposed product and sum distribution layers, the arithmetic distribution neural network is devised for background subtraction. Background subtraction is a binary classification of temporal pixels; thus, the distributions of temporal

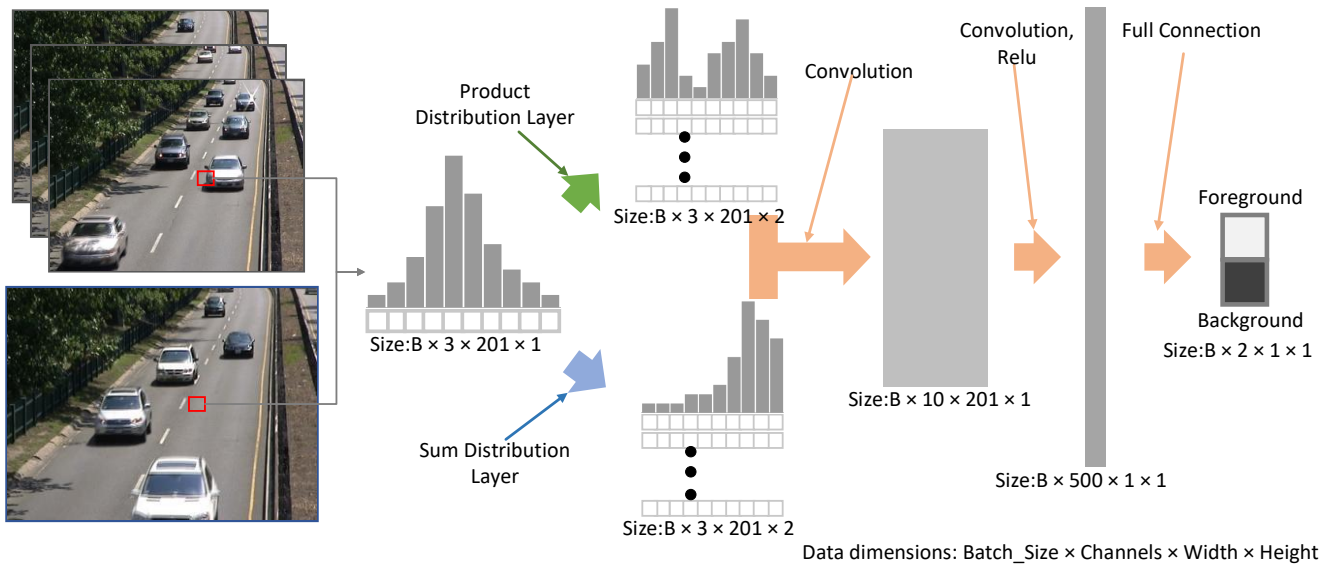


Fig. 2. An illustration of the arithmetic distribution neural network for background subtraction. Histograms of subtractions between pixels' current observation and their historical counterparts are used as input to arithmetic distribution layers for learning distributions. The output histograms of arithmetic distribution layers are combined by a convolution and input into a classification architecture containing a convolution layer, a rectified linear unit (Relu) layer, and a fully connected layer for classification.

pixels play an important role. In this work, the distributions of subtractions between pixels and their historical counterparts are used for classification. In particular, histograms are utilized to describe the distributions of subtractions and also directly used as the input of the proposed arithmetic distribution neural network. The network architecture is quite straightforward: histograms are first input into the product distribution layer and the sum distribution layer; then, the outputs of these layers are combined by a convolution followed by a classification architecture which consists of a convolution, a rectified linear unit (Relu) layer, and a fully connected layer. The classification architecture is deliberately kept as simple as possible, with only 3 layers, in order to demonstrate that the good results come from the proposed arithmetic distribution layers.

The components of the proposed arithmetic distribution neural network for background subtraction are illustrated in Fig. 2, with details of the network architecture presented in Table I. Starting with a given frame of a video, denoted as $\mathcal{I} = \{I_1, I_2, \dots, I_T\} = \{I_t | t = [1, T] \cap \mathbb{N}\}$, where t is the frame index, T the number of frames, and \mathbb{N} a natural number, to perform background subtraction for a particular pixel located at (x, y) on frame t , the histogram of the subtractions between pixels' current observation and their historical counterparts is captured for classification. Mathematically:

$$H_{x,y}(n) = \sum_{i=1}^T (I_i(x, y) - I_t(x, y)) \cap n, \quad (7)$$

where $H_{x,y}$ is the histogram of subtractions, and n is the index of entries of the histogram. $I_i(x, y)$ denotes historical observations of the pixel located at (x, y) , and $I_t(x, y)$ denotes its current observation. The distributions of subtractions are directly used as the input to the product distribution layer and the sum distribution layer for distribution learning. Then, the outputs of these two layers are combined with a convolution

TABLE I
DETAILS OF THE PROPOSED ARITHMETIC DISTRIBUTION NEURAL NETWORK ARCHITECTURE FOR BACKGROUND SUBTRACTION.

Type	Filters	Layer size	Data size
Input			$B \times 3 \times 201 \times 1$
Product Distribution	2	$3 \times 201 \times 1$	$B \times 3 \times 201 \times 2$
sum distribution	2	$3 \times 201 \times 1$	$B \times 3 \times 201 \times 2$
Convolution	10	$3 \times 1 \times 2$	$B \times 10 \times 201 \times 1$
Convolution	500	$10 \times 201 \times 1$	$B \times 500 \times 1 \times 1$
Rectified linear unit			
Convolution	2	$500 \times 1 \times 1$	$B \times 2 \times 1 \times 1$
Softmax			

B: Batch size.

procedure which is followed by the classification architecture. Mathematically:

$$\mathcal{M}(x, y) = \mathcal{L}(\mathcal{C}(\mathcal{F}_p(H_{x,y}) + \mathcal{F}_a(H_{x,y}))), \quad (8)$$

where $H_{x,y}$ is the input histogram; \mathcal{F}_p and \mathcal{F}_a denote the product distribution and the sum distribution layer; \mathcal{C} is the convolution procedure; and \mathcal{L} is the classification architecture consisting of a convolution, a rectified linear unit, and a fully connected layer. $\mathcal{M}(x, y)$ is the label of a pixel.

Unfortunately, the histograms utilized for classification are captured from independent pixels; thus, the correlation between pixels is ignored. In order to improve the accuracy of the proposed approach, an improved Bayesian refinement model is proposed. For completeness, we briefly introduce the Bayesian refinement model; please check [78] for more details. In the Bayesian refinement model, the labels of pixels are re-inferred according to the correlations with their neighborhoods, and the Bayesian theory is utilized during inference. In particular, Euclidean distance is used to compute the correlation. In contrast, we utilize a mixture of Gaussian approximation functions to capture the correlation. This is the main difference compared

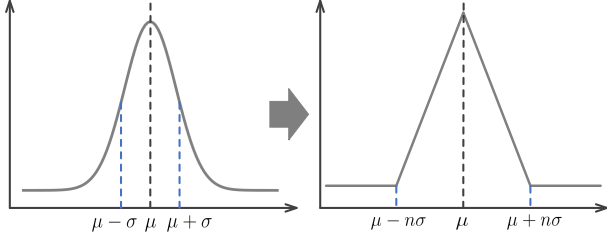


Fig. 3. An illustration of the Gaussian approximation function which approximates using a piecewise function controlled by the parameters of the Gaussian function.

to the original Bayesian refinement model. Mathematically:

$$\begin{aligned}
 \mathcal{F}(I(x, y), \mathcal{M}) &= \underset{a_i}{\operatorname{argmax}} \frac{P(I(x, y)|a_i)P(a_i)}{P(I(x, y))} \\
 &= \underset{a_i}{\operatorname{argmax}} P(a_i) \sum_{k=1}^K \pi_k \mathcal{N}_p(v_k | \mu_{k,i}, \Sigma_{k,i}) \\
 &\because P(I(x, y)) = N \\
 &\quad \& \operatorname{argmax}_x N x = \operatorname{argmax}_x x \\
 P(I(x, y)|a_i) &= \sum_{k=1}^K \pi_k \mathcal{N}_p(v_k | \mu_{k,i}, \Sigma_{k,i}),
 \end{aligned} \tag{9}$$

where \mathcal{F} is denoted as the proposed improved Bayesian refinement model. $a_i \in \{0, 1\}$ denotes the labels of foreground or background; $I(x, y)$ is a pixel located at (x, y) ; and, $P(I(x, y)|a_i)$ is the probability that the label of this pixel is a_i , which is captured through a mixture of Gaussian approximation functions $\mathcal{N}_p(v_k | \mu_{k,i}, \Sigma_{k,i})$. In particular, v_k denotes the feature vector consisting of the Lab color and spatial position of the pixel $I(x, y)$, and k is the index of entries in a vector. μ_k and Σ_k denote the mean and variance of features of a pixel in a local rectangular range with center at (x, y) and radius $R = 4$. π_k is the weight to mix the Gaussian approximation functions \mathcal{N}_p which is mathematically expressed as:

$$\mathcal{N}_p(x | \mu, \sigma) = \begin{cases} 1 + \frac{x-\mu}{n\sigma} & |x - \mu| \leq n\sigma \\ 0 & \text{otherwise} \end{cases} \tag{10}$$

where μ and σ denote the mean and variance, and n is a user parameter. During experiments, $n = 2$ gives us the best results. As shown in Fig. 3, the Gaussian approximation function is actually a rough estimate of the Gaussian function. We use a piecewise function to approximate the waveform of the Gaussian function considering the computational cost. Also, it is more convenient for a GPU implementation, which significantly accelerates the refinement procedure.

Finally, the output binary mask is used in the input again to generate better results iteratively. The Bayesian refinement model is utilized to iteratively refine the foreground mask. Mathematically:

$$\mathcal{M}_n(x, y) = \mathcal{F}(I(x, y), \mathcal{M}_{n-1}), \tag{11}$$

where n is the iteration number and \mathcal{M}_{n-1} is the binary mask from the last iteration. Using a GPU implementation, with the

TABLE II
COMPARISON BETWEEN BAYESIAN REFINEMENT MODEL AND OUR IMPROVED BAYESIAN REFINEMENT MODEL ON FRAMES OF VIDEOS WITH DIFFERENT RESOLUTIONS.

Video	Resolution	NI	BRM		IBRM	
			Time/s	Time/s	Fm value	Fm value
highway	320 × 240	1	1.2533	1.4429	0.9554	0.9612
		20	21.1842	2.2524	0.9826	0.9828
		50	52.7545	3.5712	0.9911	0.9905
canoe	320 × 240	1	1.1496	1.4215	0.9552	0.9528
		20	19.9488	2.2968	0.9535	0.9482
		50	50.4685	3.5780	0.9534	0.9453
wetSnow	720 × 540	1	5.2601	1.6945	0.7252	0.7279
		20	93.1602	5.8695	0.7731	0.7646
		50	234.7885	12.5385	0.7750	0.7732

NI: Number of iterations BRM: Bayesian refinement model
I_BRM: Improved Bayesian refinement model.

number of iterations set to 30, the entire refinement procedure only takes a few second.

The improved Bayesian refinement model (IBRM) runs much faster than the Bayesian refinement model (BRM) with almost no loss in accuracy. A comparison between them on a few frames from videos with different resolutions is shown in Table II. In particular, the running time of BRM and IBRM with iteration numbers 1, 20 and 50 are presented, as well as the Fm value of their corresponding output masks after refinement. As shown in Table II, when the number of iterations is 50, although the Fm value of output mask has obvious improvement, the run time also increases to 52s, which is too long for real applications. In contrast, IBRM needs only 3.5s in processing time, and the Fm value of the output mask is still close to the one for BRM. Thus, the superiority of the proposed IBRM is demonstrated.

V. EXPERIMENTS

A. Verification of Arithmetic Distribution Layers

In this section, we verify the correctness of the proposed arithmetic distribution layers including the product distribution layer and sum distribution layer, which are the implementations of Eqn. 3–6, respectively. In the experiments, synthetic data is used for verification. In particular, two continuous independent random variables X and W , which are described by two different probability density functions representing two histograms, are generated. In addition, the product $Z_p = XW$ and the sum $Z_s = X + W$ of the two variables X and W are computed for use as the target output. The values of X and W as well their product and sum are generated over one million times to capture the target histograms of Z_p and Z_s . The verification experiment is quite straightforward: the histogram of X is input into the product distribution layer and the sum distribution layer, respectively, to compute with the histogram of W' in layers to output the histograms of Z'_p and Z'_s . The output histograms are then compared with the target histograms of Z_p and Z_s to capture the gradients to train the arithmetic distribution layers. Finally, the correlation values between the output histograms and target histograms

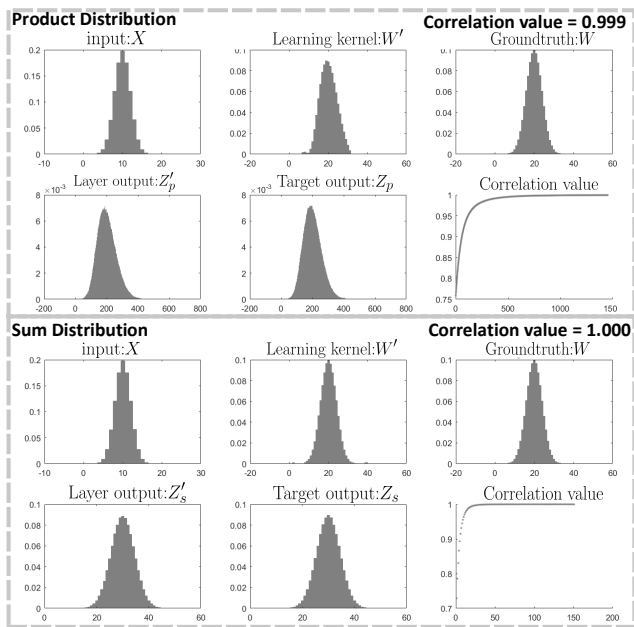


Fig. 4. Validation of the arithmetic distribution layers including product and sum distribution layers. The histogram of input X , the histogram in the learning kernel W' , the histogram of ground truth W , the histograms of layer output Z'_p and Z'_s , the target histograms of Z_p and Z_s and the correlation-epoch plot are shown.

are computed to verify if the output is close to the target. Mathematically, the correlation value is computed as:

$$v = \frac{H_Z \cdot H_{Z'}}{|H_Z| |H_{Z'}|} \quad (12)$$

where H_Z and $H_{Z'}$ are the histograms of the target distribution and output distribution, and v is the correlation value. The experimental results are shown in Fig. 4, in which the histograms of X and W , the histograms of layers output Z'_p and Z'_s , the target histograms of Z_p and Z_s , the histogram of the arithmetic distribution layers W' , and the correlation-epoch plots are shown. After training hundreds of epochs, the correlation between the output and target distributions is almost equal to 1. Furthermore, the distribution learned by the arithmetic distribution layers is almost the same as the one for W , which is used to generate the target histogram. Both of these results demonstrate that the proposed arithmetic distribution layers have the ability to output the desired distributions. The correctness of the proposed arithmetic distribution layer, which contains the forward pass and backpropagation through layers, is thus verified.

B. Comparison with a Convolutional Neural Network

In this section, the superiority of the proposed arithmetic distribution neural network (ADNN) compared to the convolutional neural network (CNN) is demonstrated. For a fair comparison, we use three CNNs for comparisons and the architectures of CNNs and ADNN are kept as similar as possible. The details of architectures are shown in Table III. In particular, the last three layers and the size of input

are kept the same in our ADNN and the compared CNNs. During comparisons several videos from the CDnet [80] dataset are extracted. In the experiments, one ground truth frame from a particular video is used as the output label of CNNs and ADNN for training. Furthermore, the distributions of differences between historical and current observations of pixels corresponding to the ground truth frame are used as the input for training. After training, the remaining frames are used for testing to demonstrate the superiority of ADNN in distribution analysis compared to CNNs. For comparison, the Re (Recall), Pr (Precision) and Fm (F-measure) metrics are used. Quantitative comparisons are shown in Table IV.

As shown in Table IV, the proposed approach achieves better Fm value for most of the videos. In the comparison between the proposed ADNN and CNN₁, since the product and sum distribution layers are the unique differences, any superiority of ADNN is attributable to our distribution arithmetic layers. In the comparison one may doubt that the number of parameters in the ADNN is greater than CNN₁, since more parameters are supposed to generate better results. However, the proposed ADNN also achieves better results compared to CNN₂ which has over 10 times the number of parameters than the proposed approach, while the depth of the proposed ADNN and CNN₂ are the same. In addition, the proposed approach achieves better results even compared to CNN₃ which contains almost 100 times the number of parameters and deeper network architecture. Hence, in a few complex videos such as “fountain02,” “backdoor,” and “bungalows,” the proposed ADNN has clear improvements compared to all three CNNs. Thus, it is fair to conclude that the proposed arithmetic distribution neural work is better for distribution classification compared to a traditional convolutional neural network.

C. Generality of Distribution Learning

The distributions of temporal pixels are relatively independent of the scene information, demonstrating that the proposed approach is generalizable. Compared to previous scene information based algorithms that need to be trained with a particular network for every video, the proposed approach is not limited by the scene information and can be trained with groups of frames obtained from different videos simultaneously. Our approach is effective even when no frame from the testing video is included in the training set. The generality of distribution information demonstrates the potential applications of the proposed approach in real applications, since a single well-trained network can be used in several different scenes with limited ground truth frames required for training. In order to demonstrate generality, we randomly select two videos as the training set in which 4 ground truth frames from each video are extracted for training, and the remaining frames are utilized for testing. Note that the ground truth frames utilized for training take less than 1% of the total ground truth frames for a video. Besides, two more new videos are also randomly selected from the dataset to test the proposed approach, under the condition that no frame from the testing video is included in the training set. In addition, in order to test the proposed approach under a more

TABLE III

DETAILS OF THE NETWORK ARCHITECTURE OF THE ARITHMETIC DISTRIBUTION NEURAL NETWORK (ADNN) AND THE CONVOLUTIONAL NEURAL NETWORKS (CNNs), USED FOR COMPARISON TO DEMONSTRATE THE SUPERIORITY OF THE PROPOSED APPROACH.

CNN ₁			CNN ₂			CNN ₃			ADNN			Data Size
Type	Filters	Size	Type	Filters	Size	Type	Filters	Size	Type	Filters	Size	
Input												B×3×201×1
			Conv	8	3×1×1	Conv	8	3×1×1				
			Conv	16	8×201×1	Conv	16	8×1×1				B×1×201×1
			Conv	16	8×201×1	Conv	32	16×201×1	ProDis	1	3×201×1	
Conv	1	3×1×1	Conv	201	16×1×1	Conv	128	32×1×1	SumDis	1	3×201×1	B×2×1×1
Relu			Conv	201	16×1×1	Conv	201	128×1×1	Conv	1	3×1×1	
Conv	2	1×201×1	Relu			Relu			Relu			
Softmax			Conv	2	1×201×1	Conv	2	1×201×1	Conv	2	1×201×1	
			Softmax			Softmax			Softmax			
NTP		405	NTP		29370	NTP		133290	NTP		1611	

ProDis: product distribution layer SumDis: sum distribution layer Conv: Convolution Relu: Rectified Linear Unit NTP: Number of total parameters
B: batch size

TABLE IV

QUANTITATIVE COMPARISON BETWEEN CNNs AND ADNN USING RE, PR, AND FM METRICS BASED ON REAL DATA.

Videos	CNN ₁			CNN ₂			CNN ₃			ADNN		
	Re	Pr	Fm	Re	Pr	Fm	Re	Pr	Fm	Re	Pr	Fm
highway	(0.9086 , 0.8133 , 0.8583)	(0.8732 , 0.7599 , 0.8126)	(0.9532 , 0.8017 , 0.8709)	(0.9603 , 0.8697 , 0.9127)								
pedestrians	(0.9370 , 0.9404 , 0.9387)	(0.9536 , 0.9062 , 0.9293)	(0.9474 , 0.8942 , 0.9201)	(0.9399 , 0.9690 , 0.9542)								
fountain01	(0.1404 , 0.1988 , 0.1646)	(0.6434 , 0.4435 , 0.5250)	(0.5944 , 0.5001 , 0.5432)	(0.5953 , 0.5311 , 0.5613)								
canoe	(0.8134 , 0.8398 , 0.8264)	(0.9464 , 0.9532 , 0.9498)	(0.9439 , 0.9663i , 0.9550)	(0.9450 , 0.9654 , 0.9551)								
fountain02	(0.7289 , 0.8812 , 0.7978)	(0.7850 , 0.8584 , 0.8201)	(0.7670 , 0.9186 , 0.8360)	(0.7738 , 0.9534 , 0.8543)								
peopleInShade	(0.9893 , 0.2478 , 0.3963)	(0.9054 , 0.4649 , 0.6144)	(0.8941 , 0.4758 , 0.6211)	(0.9808 , 0.4542 , 0.6209)								
backdoor	(0.7665 , 0.5195 , 0.6192)	(0.9275 , 0.2987 , 0.4519)	(0.9033 , 0.3420 , 0.4962)	(0.9134 , 0.5555 , 0.6908)								
traffic	(0.6881 , 0.9008 , 0.7802)	(0.7009 , 0.9541 , 0.8081)	(0.7167 , 0.9499 , 0.8170)	(0.6927 , 0.9670 , 0.8072)								
sidewalk	(0.5490 , 0.3675 , 0.4403)	(0.8392 , 0.3368 , 0.4807)	(0.8314 , 0.3587 , 0.5012)	(0.7851 , 0.3437 , 0.4781)								
busStation	(0.8587 , 0.7870 , 0.8212)	(0.8846 , 0.8297 , 0.8563)	(0.8913 , 0.8544 , 0.8725)	(0.9097 , 0.9057 , 0.9077)								
bungalows	(0.8636 , 0.9604 , 0.9094)	(0.8535 , 0.9607 , 0.9039)	(0.8493 , 0.9649 , 0.9034)	(0.9073 , 0.9788 , 0.9417)								
library	(0.9101 , 0.9702 , 0.9392)	(0.9075 , 0.9701 , 0.9378)	(0.9193 , 0.9444 , 0.9444)	(0.9358 , 0.9746 , 0.9548)								
Average	(0.7628 , 0.7022 , 0.7076)	(0.8517 , 0.7280 , 0.7575)	(0.8509 , 0.7476 , 0.7734)	(0.8616 , 0.7890 , 0.8032)								

complex condition, the number of training and testing videos is increased to four. Four videos from different categories are selected as the training set in which four ground truth frames from each are extracted for training and the remaining frames are used for testing. Similarly, four more new videos are also randomly selected to evaluate the proposed approach. Quantitative and qualitative experiments are shown in Table V and Fig. 5, respectively.

As shown in Table V, the proposed approach is trained well when frames from different scenes are combined as the training set and achieves good performance during the testing on the remaining frames. For example, the proposed ADNN is trained by frames captured from videos “highway” and “pedestrians,” and achieves 0.9891 and 0.9572 in Fm values. It is effective even when the unseen videos “office” and “PETS2006” are used for testing. Furthermore, the proposed approach still achieves good results when the training frames are captured from four videos, which are randomly selected from different categories. As shown in Fig. 5, when the scene information of four videos that produce the training frames are completely different, the proposed approach is still well-trained with the input using the ground truth frames from these different videos. Also, the proposed approach achieves good results when another four unseen videos from different categories are used for testing. In conclusion, the proposed approach can be trained with image frames with different scene information, and it is effective even when unseen videos

are utilized for testing. Thus, the generality of the proposed approach is demonstrated.

TABLE V

QUANTITATIVE GENERALITY EVALUATION OF THE PROPOSED APPROACH USING RE, PR AND FM METRICS.

	Training Sets		Testing Sets		Performance		
	Category	Video	Category	Video	Re	Pr	Fm
The same category	Baseline	highway	Baseline	highway	(0.9968, 0.9814, 0.9891)		
		pedestrians	Baseline	pedestrians	(0.9891, 0.9274, 0.9572)		
		office	Baseline	office	(0.8435, 0.8256, 0.8345)		
		PETS2006	Baseline	PETS2006	(0.9395, 0.8367, 0.8851)		
	Dyn. Bg.	fountain01	Dyn. Bg.	fountain01	(0.8268, 0.8102, 0.8184)		
		overpass	Dyn. Bg.	overpass	(0.9961, 0.9398, 0.9671)		
		canoe	Dyn. Bg.	canoe	(0.9689, 0.9366, 0.9524)		
		fountain02	Dyn. Bg.	fountain02	(0.9794, 0.7536, 0.8518)		
Different categories	Baseline	highway	Baseline	highway	(0.9937, 0.9915, 0.9926)		
		bungalows	Shadow	bungalows	(0.9989, 0.9767, 0.9877)		
		canoe	Dyn. Bg.	canoe	(0.9708, 0.9663, 0.9686)		
		overpass	Dyn. Bg.	overpass	(0.9968, 0.9276, 0.9610)		
	Dyn. Bg.	office	Baseline	office	(0.8404, 0.9400, 0.8874)		
		peopleInShade	Shadow	peopleInShade	(0.9835, 0.9794, 0.9814)		
		fountain02	Dyn. Bg.	fountain02	(0.9864, 0.7913, 0.8781)		
		boats	Dyn. Bg.	boats	(0.9700, 0.9361, 0.9527)		
	Low Fr.	fountain01	Dyn. Bg.	fountain01	(0.8476, 0.8122, 0.8295)		
		tramCross.	Low Fr.	tramCross.	(0.9611, 0.8805, 0.9190)		
		library	Ther.	library	(0.9467, 0.9892, 0.9675)		
		skating	Bad Wea.	skating	(0.9639, 0.9831, 0.9734)		
Bad Wea.	pedestrians	Baseline	pedestrians	(0.9903, 0.8473, 0.9133)			
	canoe	Dyn. Bg.	canoe	(0.9775, 0.8674, 0.9191)			
	corridor	Ther.	corridor	(0.7651, 0.9077, 0.8303)			
	bungalows	Shadow	bungalows	(0.9725, 0.9802, 0.9764)			

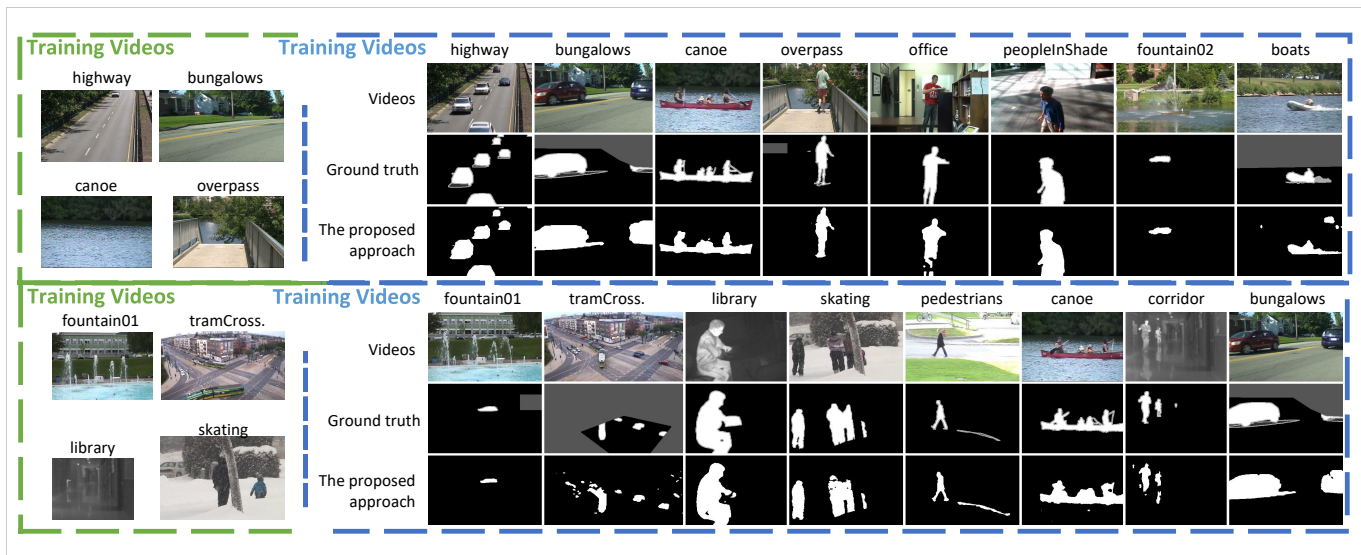


Fig. 5. Qualitative generality evaluation of the proposed approach.

TABLE VI
QUANTITATIVE COMPARISON BETWEEN THE PROPOSED APPROACH AND STATE-OF-THE-ART METHODS, USING FM METRIC ON THE LASIESTA [81] DATASET.

Videos	ADNN-IBRM	D-DPDL [78]	CueV2 [82]	Hai [8]	Cue [83]
I_SI_01	0.9764	0.9596	0.9208	0.9622	0.8143
I_SI_02	0.9309	0.8687	0.8403	0.8130	0.7576
I_CA_01	0.9807	0.9309	0.9062	0.9220	0.8424
I_CA_02	0.9201	0.8850	0.7826	0.8656	0.6296
I_OC_01	0.9783	0.9710	0.7013	0.8920	0.8274
I_OC_02	0.9735	0.9677	0.8600	0.9526	0.8781
I_IL_01	0.7702	0.7161	0.6452	0.8861	0.7966
I_IL_02	0.7620	0.8972	0.6523	0.8122	0.7864
I_MB_01	0.9874	0.9699	0.9543	0.9816	0.7779
I_MB_02	0.9731	0.9195	0.9204	0.7064	0.6797
I_BS_01	0.9787	0.8371	0.7132	0.6285	0.5065
I_BS_02	0.9626	0.6178	0.6156	0.7333	0.6607
O_CL_01	0.9840	0.9792	0.9508	0.6946	0.9280
O_CL_02	0.9788	0.9800	0.9045	0.9588	0.8995
O_RA_01	0.9896	0.9072	0.8453	0.8225	0.7462
O_RA_02	0.9839	0.9803	0.8886	0.9590	0.8699
O_SN_01	0.9733	0.9690	0.9317	0.3054	0.8214
O_SN_02	0.9562	0.9341	0.6256	0.0426	0.0895
O_SU_01	0.9186	0.9065	0.6774	0.8115	0.6527
O_SU_02	0.9413	0.9388	0.7669	0.9021	0.8074
Average	0.9460	0.9068	0.8051	0.7826	0.7386

D. Evaluation of Arithmetic Distribution for Background Subtraction

In this section, a comprehensive evaluation of the proposed approach is presented through comparisons with several state-of-the-art methods including deep learning networks on the LASIESTA [81] and CDnet2014 [80] datasets. To the best of our knowledge, after the rise of deep learning networks in the background subtraction field, the fairness of comparisons between deep learning methods has been a concern. It is commonly accepted that the quantity of training data and the number of parameters in a network have significant and direct contribution to the performance of various methods [91]; but, the assumptions of training data, numbers of parameters in the network and the utilization of pre-trained networks in

these methods are completely different. A few methods have generated almost perfect results with the assumption of a large number of ground truth frames for training. For example, FgSegNet model [92] achieves over 99% in Fm value on the CDnet Dataset [80], when 200 frames of ground-truth mask from each video are extracted for training and over hundreds of millions of parameters are used in the network. Such algorithms did achieve better results than the proposed approach. However, the comparison between FgSegNet and the proposed approach is unfair, since we only use 20 ground truth frames for training and the number of parameters in our network is much less than their network. In addition, there are a few semi-supervised algorithms (e.g., GuidedBS [53], BSUV-Net [90] and GraphMOS [56]) which did not utilize any ground truth frames from testing videos for training. However, these methods assumed a large number of binary masks from another video for training, and used several pre-trained networks. For example, VGG-16 [93] or Mask R-CNN [94] are combined into their network. It should be noted that these pre-trained networks still need a significant amount of data for training. For instance, GraphMOS [56] employed Mask R-CNN network [94] and DeepLab network [95] in their network, and both of these two networks were well trained with a large number of masks for objects segmentation or semantic segmentation which are similar to the ground masks of background subtraction. In contrast, the proposed approach does not use any pre-trained models or extra training data from others datasets. The comparison between the proposed approach and GraphMOS model is also questionable. GraphMOS is devised for unseen videos but many training frames may already contain information from testing videos; and although the proposed approach only assumes less than 1 % of ground truth frames for training, such frames are still extracted from testing videos. Thus, before the comparison between the proposed approach and other compared algorithms, the training data and pre-trained networks utilized in algorithms are discussed. The proposed approach is compared

TABLE VII
QUANTITATIVE COMPARISON BETWEEN THE PROPOSED APPROACH AND STATE-OF-THE-ART METHODS, USING THE FM METRIC ON THE CDNET2014 [80] DATASET.

Approach	Baseline	Dyn. Bg.	Cam. Jitt.	Int. Mot.	Shadow	Ther.	Bad Wea.	Low Fr.	Nig. Vid.	PTZ	Turbul.	Overall	
IUTIS-5 [13]	0.9567	0.8902	0.8332	0.7296	0.9084	0.8303	0.8248	0.7743	0.5290	0.4282	0.7836	0.7717	
MBS [84]	0.9287	0.7915	0.8367	0.7568	0.7968	0.8194	0.7980	0.6350	0.5158	0.5520	0.5858	0.7288	
PAWCS [85]	0.9397	0.8938	0.8137	0.7764	0.8913	0.8324	0.8152	0.6588	0.4152	0.4615	0.6450	0.7403	
ShareM [14]	0.9522	0.8222	0.8141	0.6727	0.8898	0.8319	0.8480	0.7286	0.5419	0.3860	0.7339	0.7474	
SuBSENSE [15]	0.9503	0.8177	0.8152	0.6569	0.8986	0.8171	0.8619	0.6445	0.5599	0.3476	0.7792	0.7408	
WeSamBE [28]	0.9413	0.7440	0.7976	0.7392	0.8999	0.7962	0.8608	0.6602	0.5929	0.3844	0.7737	0.7446	
GMM [4]	0.8245	0.6330	0.5969	0.5207	0.7370	0.6621	0.7380	0.5373	0.4097	0.1522	0.4663	0.5707	
RMoG [7]	0.7848	0.7352	0.7010	0.5431	0.7212	0.4788	0.6826	0.5312	0.4265	0.2470	0.4578	0.5735	
3PDM [86]	0.8820	0.8990	0.7270	0.6860	0.8650	0.8410	0.8280	0.5350	0.4210	0.5010	0.7930	0.7253	
HMAO [87]	0.8200	N/A	0.6300	0.7200	0.8600	0.8400	0.7900	0.6000	0.3600	N/A	0.4600	N/A	
B-SSSR [26]	0.9700	0.9500	0.9300	0.7400	0.9300	0.8600	0.9200	N/A	N/A	N/A	0.8700	N/A	
MSCL-FL [25]	0.9400	0.9000	0.8600	0.8400	0.8600	0.8600	0.8800	N/A	N/A	N/A	N/A	N/A	
DSPSS [88]	0.9664	0.9057	0.8662	0.7870	0.9177	0.7328	N/A	N/A	N/A	N/A	N/A	N/A	
STSHBM [59]	0.9534	0.9120	0.8503	0.8349	0.8930	0.8579	N/A	N/A	N/A	N/A	N/A	N/A	
DPGMM [8]	0.9286	0.8137	0.7477	0.5418	0.8127	0.8134	N/A	N/A	N/A	N/A	N/A	N/A	
deep learning methods	BMN-BSN [89]	0.9521	0.6371	0.6962	0.6369	0.7893	0.7849	0.8124	0.6426	0.6125	N/A	N/A	N/A
	DeepBS [52]	0.9580	0.8761	0.8990	0.6098	0.9304	0.7583	0.8301	0.6002	0.5835	0.3133	0.8455	0.7548
	GuidedBS [53]	0.9467	0.8266	0.8818	0.6229	0.8910	0.7490	0.8711	0.6396	0.5048	0.6057	0.8114	0.7591
	CNN-SFC [54]	0.9497	0.9035	0.8035	0.7499	0.9127	0.8494	0.9084	0.7808	0.6527	0.7280	0.8288	0.8243
	CwisarDH [38]	0.9145	0.8274	0.7886	0.5753	0.8581	0.7866	0.6837	0.6406	0.3735	0.3218	0.7227	0.6812
	DPDL ₄₀ [77]	0.9692	0.8692	0.8661	0.8759	0.9361	0.8379	0.8688	0.7078	0.6110	0.6087	0.7636	0.8106
	D-DPDL ₁₀ [78]	0.9743	0.9008	0.9098	0.8887	0.9526	0.8808	0.9001	0.7527	0.6505	0.6362	0.8073	0.8413
	GraphMOS [56]	0.9710	0.8922	0.9233	0.6455	0.9901	0.9010	0.9411	0.6910	0.8211	0.8511	0.8233	0.8592
	BSUV-Net [90]	0.9640	0.8176	0.7788	0.7601	0.9664	0.8455	0.8730	0.6788	0.6815	0.6562	0.7631	0.7986
	DVTN [57]	0.9811	0.9329	0.9014	0.9595	0.9467	0.9479	0.8780	0.7818	0.7737	0.5957	0.9034	0.8789
ADNN	0.9729	0.9110	0.8997	0.8857	0.9305	0.9091	0.8512	0.7370	0.6215	0.6310	0.8405	0.8355	
ADNN-IBRM	0.9797	0.9454	0.9411	0.9114	0.9537	0.9411	0.9038	0.8123	0.6940	0.7424	0.8806	0.8826	

with several state-of-the-art algorithms based on deep learning networks, containing DeepBS [52], GuidedBS [53], CNN-SFC [54], CwisarDH [38], DPDL model [77], D-DPDL model [78], GraphMOS [56], BSUV-Net [90], DVTN [57] and BMN-BSN [89]. In particular, DeepBS [52] used 5% of ground truth frames of the entire dataset. GuidedBS [53] used 200 foreground images generated by SubSENSE [15]. DVTN [57] extracted 100 ground truth frames from each video for training. CNN-SFC [54] utilized 4,000 ground truth frames of the testing dataset and a pre-trained VGG network which is trained on the Imagenet dataset [96]. GraphMOS [56] used 350 ground truth frames from other videos for training and several pre-trained instance segmentation networks including Res-Net [97], Mask R-CNN [94] and DeepLab network [95]. BMN-BSN [89] required 30,000 ground truth frames for training. BSUV-Net [90] assumed 200 frames from unseen videos for training and a pre-trained network from DeepLabv3 [98] using 20,000 images with dense annotations is utilized. DPDL [77] and D-DPDL [78] randomly extracted 40 and 10 ground truth frames, respectively, from each video of the CDnet [80] dataset. Unfortunately, there is a lack of training details about CwisarDH [38]. All of the training details and the compared results are directly obtained from the paper and implementation provided by the authors. For the proposed approach, 20 ground truth frames from each video are used for training. More training details are discussed during comparisons.

The quantitative evaluation of the proposed ADNN incorporating the improved Bayesian refinement model (ADNN-IBRM) on the LASIESTA [81] dataset is shown in Table VI. During the evaluation, both the proposed approach and the D-DPDL model randomly extracted 3 ground truth frames

of each video for training. This takes only 0.72% of the ground truth frames available in the LASIESTA [81] dataset. As shown in Table VI, the proposed approach achieves better results in almost all these videos compared to D-DPDL [78], since the proposed approach learns the entire histogram rather than an expected value of the histogram. Unfortunately, the proposed ADNN-IBRM does not work very well for the videos “I_IL_01” and “I_IL_02.” In these videos, the illumination varies over time, but only 3 ground truth frames are randomly selected during training. The quantity of training frames is very small. Thus, it is possible that the time intervals of training frames are very short, and the information on global illumination change is not included in the training frames. This results in the poor results of the proposed approach.

Quantitative and qualitative evaluations of the proposed approach on the CDnet2014 [80] dataset are shown in Table VII and Fig. 6, respectively. In particular, ADNN demonstrates the results of the proposed approach without improved Bayesian refinement model, and ADNN-IBRM presents the results of the complete proposed approach. The number of parameters of our ADNN is around 1 million, which is much less than the ones for other compared methods based on deep learning networks. In addition, no pre-trained network or extra training data is utilized in the proposed approach. The details of network architecture of the proposed approach is shown in Table I. During the training of the proposed approach, 20 ground truth frames of each video are extracted for training. This only takes 0.66% of the entire dataset. Also, since less than 1% of ground truth frames are utilized for training, the proposed approach can be compared even with unsupervised approaches, such as B-SSSR [26], which we assume to be the

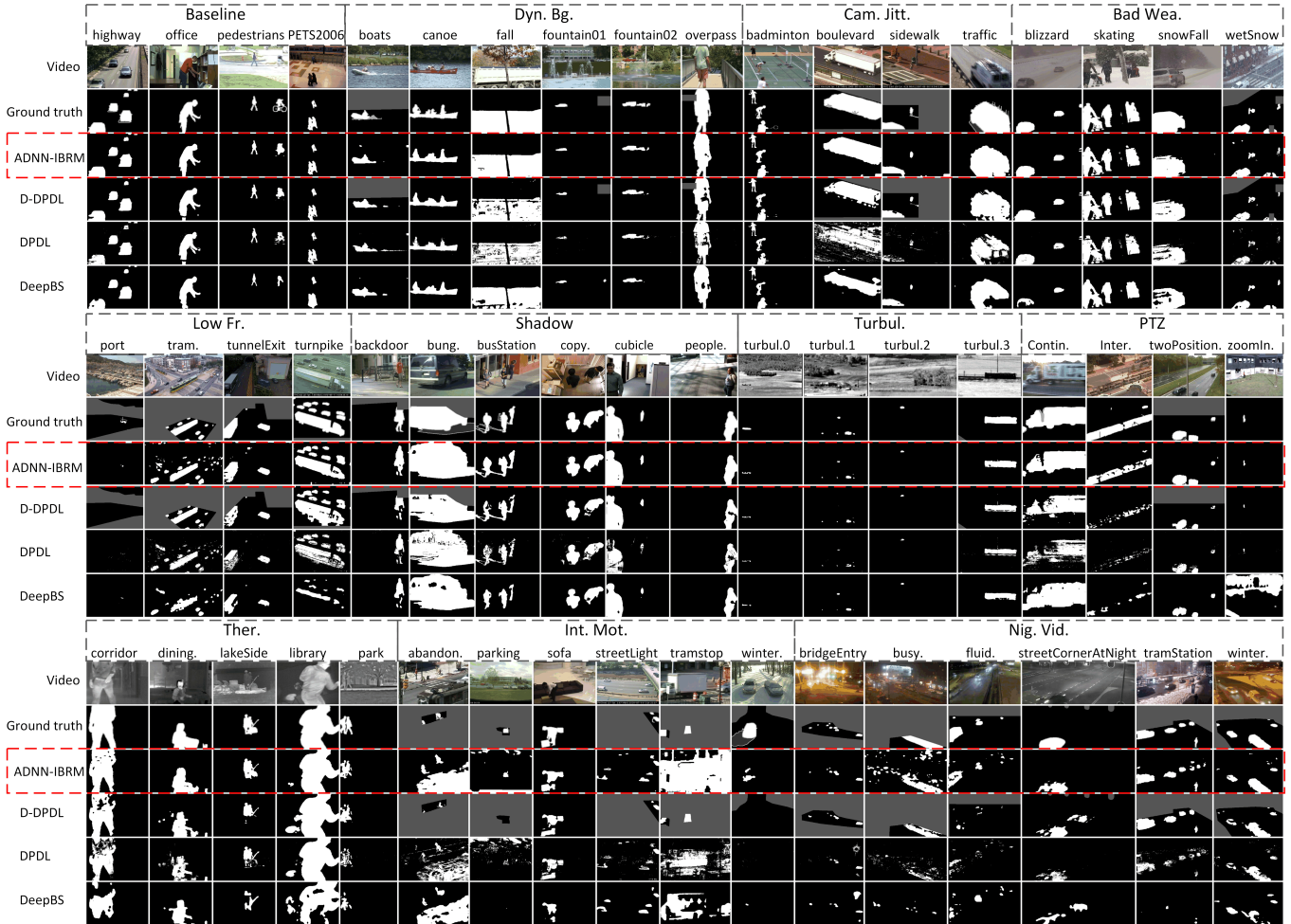


Fig. 6. Qualitative comparison between the proposed approach and several state-of-the-art methods, including D-DPDL [78], DPDL [77] and DeepBS [52] on the CDnet2014 [80] dataset.

best unsupervised method.

As shown in Table VII, the proposed ADNN-IBRM has the best overall performance compared to both unsupervised and supervised methods. The ADNN excluding the improved Bayesian refinement model also achieves promising results. Actually, most methods based on deep learning networks are promising. However, it should be noted again that all of these methods assume much more ground truth masks than the proposed approach. Also, the number of parameters in these other networks are much greater than the proposed approach. Unfortunately, the proposed approach does not produce good results for videos in the “nightVideos” (Nig. Vid.) and “PTZ” categories. The intensity of pixels in the “nightVideos” category is very low; the pixels are too dark and do not generate enough distribution information for learning. Thus, the proposed approach only achieves 0.69 on the Fm metric. Videos in the “PTZ” category are obtained by a moving camera, but the motion of the camera is not large. Hence, the distributions of temporal pixels can be used in a short time interval, which can be learned. Thus, the proposed approach achieves a 0.74 Fm value.

The proposed approach is implemented in Pytoch [79], and the source code will be made available following acceptance

of our paper. Experiments are run on a GeForce GTX 1080 GPU processor with 8 GB memory. During training 60 epochs are set as the maximum, the learning rate is set to 0.0001 and the Adam method [99] with default parameters is used for training.

VI. CONCLUSION

We proposed the Arithmetic Distribution Neural Network (ADNN) for background subtraction. Specifically, the arithmetic distribution layers, including the product and sum distribution layers, based on arithmetic distribution operations are proposed for learning the distributions of temporal pixels. Also, an improved Bayesian refinement model, based on neighborhood information with a GPU implementation, is proposed to improve the robustness and accuracy of the proposed approach. Utilizing the arithmetic distribution layers, histograms are considered as probability density functions. This probability information is used during the learning procedure of the proposed approach. Moreover, since the distribution of temporal pixels is relatively independent of the scene information, the proposed approach is effective even when the training and testing frames are acquired from different videos. Comprehensive evaluations comparing with

state-of-the-art methods showed the superior performance of the proposed approach, and demonstrated its potential for use in practical applications.

REFERENCES

- [1] M. D. Springer, "The algebra of random variables," Tech. Rep., 1979.
- [2] O. Barnich and M. Van Droogenbroeck, "Vibe: A universal background subtraction algorithm for video sequences," *IEEE Trans. Image Process.*, 2011.
- [3] D.-S. Lee, "Effective gaussian mixture learning for video background subtraction," *IEEE Trans. Pattern Anal. Mach. Intell.*, 2005.
- [4] Z. Zivkovic, "Improved adaptive gaussian mixture model for background subtraction," in *Int. Conf. Pattern Recognit. (ICPR)*, 2004.
- [5] L. Li, W. Huang, I. Y.-H. Gu, and Q. Tian, "Statistical modeling of complex backgrounds for foreground object detection," *IEEE Trans. Image Process.*, 2004.
- [6] C. R. Jung, "Efficient background subtraction and shadow removal for monochromatic video sequences," *IEEE Trans. Multimedia*, no. 3, pp. 571–577, April 2009.
- [7] S. Varadarajan, P. Miller, and H. Zhou, "Spatial mixture of Gaussians for dynamic background modelling," in *Proc. IEEE Int. Conf. Advanced Video and Signal Based Surveillance*, 2013, pp. 63–68.
- [8] T. S. F. Haines and T. Xiang, "Background subtraction with dirichlet-process mixture models," *IEEE Trans. Pattern Anal. Mach. Intell.*, no. 4, pp. 670–683, April 2014.
- [9] P. Tiefenbacher, M. Hofmann, D. Merget, and G. Rigoll, "Pid-based regulation of background dynamics for foreground segmentation," in *IEEE Int. Conf. Image Process. (ICIP)*, Oct 2014, pp. 3282–3286.
- [10] R. Wang, F. Bunyak, G. Seetharaman, and K. Palaniappan, "Static and moving object detection using flux tensor with split gaussian models," in *IEEE Conf. Comput. Vis. Pattern Recognit. Workshops (CVPRW)*, June 2014, pp. 420–424.
- [11] G. Ramírez-Alonso and M. I. Chacón-Murguía, "Auto-adaptive parallel som architecture with a modular analysis for dynamic object segmentation in videos," *Neurocomputing*, pp. 990 – 1000, 2016.
- [12] D. Liang, S. Kaneko, M. Hashimoto, K. Iwata, and X. Zhao, "Co-occurrence probability-based pixel pairs background model for robust object detection in dynamic scenes," *Pattern Recognit.*, no. 4, pp. 1374 – 1390, 2015.
- [13] S. Bianco, G. Ciocca, and R. Schettini, "How far can you get by combining change detection algorithms?" in *Int. Conf. Image Analysis and Process.*, 2017.
- [14] Y. Chen, J. Wang, and H. Lu, "Learning sharable models for robust background subtraction," in *IEEE Int. Conf. Multimedia and Expo (ICME)*, June 2015, pp. 1–6.
- [15] P. L. St-Charles, G. A. Bilodeau, and R. Bergevin, "Subsense: A universal change detection method with local adaptive sensitivity," *IEEE Trans. Image Process.*, no. 1, pp. 359–373, Jan 2015.
- [16] X. Liu, J. Yao, X. HONG, X. Huang, Z. Zhou, C. Qi, and G. Zhao, "Background subtraction using spatio-temporal group sparsity recovery," *IEEE Trans. Circuits Syst. Video Technol.*, no. 99, pp. 1–1, 2017.
- [17] H. Yong, D. Meng, W. Zuo, and L. Zhang, "Robust online matrix factorization for dynamic background subtraction," *IEEE Trans. Pattern Anal. Mach. Intell.*, July 2018.
- [18] S. Minaee and Y. Wang, "An admm approach to masked signal decomposition using subspace representation," *IEEE Trans. Image Process.*, July 2019.
- [19] T. Bouwmans, F. El Baf, and B. Vachon, "Statistical background modeling for foreground detection: A survey," in *Handbook of pattern recognition and computer vision*. World Scientific, 2010.
- [20] K. Goyal and J. Singhai, "Review of background subtraction methods using gaussian mixture model for video surveillance systems," *Artificial Intelligence Review*, 2018.
- [21] —, "Review of background subtraction methods using gaussian mixture model for video surveillance systems," *Artificial Intelligence Review*, Jan 2017.
- [22] C. Stauffer and W. Grimson, "Adaptive background mixture models for real-time tracking," in *Proc. IEEE Conf. Comput. Vis. Pattern Recognit.*, 1999, pp. –252 Vol. 2.
- [23] K. Kim, T. Chalidabhongse, D. Harwood, and L. Davis, "Background modeling and subtraction by codebook construction," in *Int. Conf. Image Process. (ICIP)*, Oct 2004, pp. 3061–3064.
- [24] E. J. Candès, X. Li, Y. Ma, and J. Wright, "Robust principal component analysis?" *J. ACM*, no. 3, Jun. 2011.
- [25] S. Javed, A. Mahmood, T. Bouwmans, and S. K. Jung, "Background-foreground modeling based on spatiotemporal sparse subspace clustering," *IEEE Trans. Image Process.*, Dec 2017.
- [26] S. Javed, A. Mahmood, S. Al-Maadeed, T. Bouwmans, and S. K. Jung, "Moving object detection in complex scene using spatiotemporal structured-sparse rpca," *IEEE Trans. Image Process.*, Feb 2019.
- [27] T. Huynh-The, O. Banos, S. Lee, B. H. Kang, E. S. Kim, and T. Le-Tien, "Nic: A robust background extraction algorithm for foreground detection in dynamic scenes," *IEEE Trans. Circuits Syst. Video Technol.*, no. 7, pp. 1478–1490, July 2017.
- [28] S. Jiang and X. Lu, "Wesambe: A weight-sample-based method for background subtraction," *IEEE Trans. Circuits Syst. Video Technol.*, no. 99, pp. 1–1, 2017.
- [29] B. Garcia-Garcia, T. Bouwmans, and A. J. Rosales Silva, "Background subtraction in real applications: Challenges, current models and future directions," *Computer Science Review*, vol. 35, p. 100204, 2020.
- [30] H.-H. Lin, T.-L. Liu, and J.-H. Chuang, "A probabilistic svm approach for background scene initialization," in *Int. Conf. Image Process. (ICIP)*, June 2002, pp. 893–896 vol.3.
- [31] L. Cheng and M. Gong, "Realtime background subtraction from dynamic scenes," in *Int. Conf. Comput. Vis. (ICCV)*, Sept 2009, pp. 2066–2073.
- [32] B. Han and L. Davis, "Density-based multifeature background subtraction with support vector machine," *IEEE Trans. Pattern Anal. Mach. Intell.*, no. 5, pp. 1017–1023, May 2012.
- [33] X. Zhang, Z. Liu, H. Li, X. Zhao, and P. Zhang, "Statistical background subtraction based on imbalanced learning," in *IEEE Int. Conf. Multimedia and Expo (ICME)*, July 2014, pp. 1–6.
- [34] X. Zhang, C. Zhu, H. Wu, Z. Liu, and Y. Xu, "An imbalance compensation framework for background subtraction," *IEEE Trans. Multimedia*, no. 11, pp. 2425–2438, Nov 2017.
- [35] D. Culibrk, O. Marques, D. Socek, H. Kalva, and B. Furht, "Neural network approach to background modeling for video object segmentation," *IEEE Trans. Neural Networks*, no. 6, pp. 1614–1627, Nov 2007.
- [36] X. Zhou, C. Yang, and W. Yu, "Moving object detection by detecting contiguous outliers in the low-rank representation," *IEEE Trans. Pattern Anal. Mach. Intell.*, no. 3, pp. 597–610, March 2013.
- [37] B.-H. Do and S.-C. Huang, "Dynamic background modeling based on radial basis function neural networks for moving object detection," in *IEEE Int. Conf. Multimedia and Expo (ICME)*, July 2011, pp. 1–4.
- [38] M. D. Gregorio and M. Giordano, "Change detection with weightless neural networks," in *IEEE Conf. Comput. Vis. Pattern Recognit. Workshops (CVPRW)*, June 2014, pp. 409–413.
- [39] L. Maddalena and A. Petrosino, "A self-organizing approach to background subtraction for visual surveillance applications," *IEEE Trans. Image Process.*, no. 7, pp. 1168–1177, July 2008.
- [40] L. Maddalena and A. Petrosino, "The sob's algorithm: What are the limits?" in *IEEE Conf. Comput. Vis. Pattern Recognit. Workshops (CVPRW)*, June 2012, pp. 21–26.
- [41] Y. Yang, T. Zhang, J. Hu, D. Xu, and G. Xie, "End-to-end background subtraction via a multi-scale spatio-temporal model," *IEEE Access*, 2019.
- [42] M. Mandal, V. Dhar, A. Mishra, S. K. Vipparthi, and M. Abdel-Mottaleb, "3dcd: Scene independent end-to-end spatiotemporal feature learning framework for change detection in unseen videos," *IEEE Transactions on Image Processing*, vol. 30, pp. 546–558, 2021.
- [43] M. Mandal and S. K. Vipparthi, "Scene independency matters: An empirical study of scene dependent and scene independent evaluation for cnn-based change detection," *IEEE Transactions on Intelligent Transportation Systems*, pp. 1–14, 2020.
- [44] W. Zheng, K. Wang, and F.-Y. Wang, "A novel background subtraction algorithm based on parallel vision and bayesian gans," *Neurocomputing*, pp. 178 – 200, 2020.
- [45] M. Sultana, A. Mahmood, T. Bouwmans, and S. K. Jung, "Dynamic background subtraction using least square adversarial learning," in *IEEE Conf. on Image Process. (ICIP)*, 2020.
- [46] M. Sultana, A. Mahmood, T. Bouwmans, and S. K. Jung, "Unsupervised adversarial learning for dynamic background modeling," in *Frontiers of Computer Vision*, 2020, pp. 248–261.
- [47] Y. Wang, Z. Luo, and P.-M. Jodoin, "Interactive deep learning method for segmenting moving objects," *Pattern Recognit. Letters*, 2016.
- [48] L. A. Lim and H. Y. Keles, "Foreground segmentation using convolutional neural networks for multiscale feature encoding," *Pattern Recognit. Letters*, pp. 256 – 262, 2018.
- [49] T. Bouwmans, S. Javed, M. Sultana, and S. K. Jung, "Deep neural network concepts for background subtraction: a systematic review and comparative evaluation," *Neural Networks*, pp. 8 – 66, 2019.
- [50] D. Zeng and M. Zhu, "Background subtraction using multiscale fully convolutional network," *IEEE Access*, 2018.

- [51] M. Braham and M. V. Droogenbroeck, "Deep background subtraction with scene-specific convolutional neural networks," in *Int. Conf. Systems, Signals and Image Process. (IWSSIP)*, May 2016, pp. 1–4.
- [52] M. Babae, D. T. Dinh, and G. Rigoll, "A deep convolutional neural network for video sequence background subtraction," *Pattern Recognit.*, pp. 635 – 649, 2018.
- [53] X. Liang, S. Liao, X. Wang, W. Liu, Y. Chen, and S. Z. Li, "Deep background subtraction with guided learning," in *IEEE Int. Conf. Multimedia and Expo (ICME)*, July 2018.
- [54] A. K. Dongdong Zeng, Ming Zhu, "Combining background subtraction algorithms with convolutional neural network," *Journal of Electronic Imaging*, no. 1, pp. 1 – 6 – 6, 2019.
- [55] R. Huang, M. Zhou, Y. Xing, Y. Zou, and W. Fan, "Change detection with various combinations of fluid pyramid integration networks," *Neurocomputing*, vol. 437, pp. 84–94, 2021.
- [56] J. H. Giraldo, S. Javed, and T. Bouwmans, "Graph moving object segmentation," *IEEE Transactions on Pattern Analysis and Machine Intelligence*, pp. 1–1, 2020.
- [57] Y. Ge, J. Zhang, X. Ren, C. Zhao, J. Yang, and A. Basu, "Deep variation transformation network for foreground detection," *IEEE Transactions on Circuits and Systems for Video Technology*, pp. 1–1, 2020.
- [58] T. S. F. Haines and T. Xiang, "Background subtraction with dirichlet processes," in *Eur. Conf. Comput. Vis. (ECCV)*. Springer Berlin Heidelberg, 2012, pp. 99–113.
- [59] M. Chen, X. Wei, Q. Yang, Q. Li, G. Wang, and M. Yang, "Spatiotemporal gmm for background subtraction with superpixel hierarchy," *IEEE Trans. Pattern Anal. Mach. Intell.*, June 2018.
- [60] M. Chen, Q. Yang, Q. Li, G. Wang, and M.-H. Yang, "Spatiotemporal background subtraction using minimum spanning tree and optical flow," in *Eur. Conf. Comput. Vis. (ECCV)*, 2014, pp. 521–534.
- [61] T. Akilan, Q. J. Wu, and Y. Yang, "Fusion-based foreground enhancement for background subtraction using multivariate multi-model gaussian distribution," *Information Sciences*, pp. 414 – 431, 2018.
- [62] F. Cheng, S. Huang, and S. Ruan, "Advanced background subtraction approach using laplacian distribution model," in *2010 IEEE International Conference on Multimedia and Expo*, 2010, pp. 754–759.
- [63] "Modeling pixel process with scale invariant local patterns for background subtraction in complex scenes," in *Proc. IEEE Conf. Comput. Vis. Pattern Recognit. (CVPR)*, 2010, pp. 1301–1306.
- [64] G. Gemignani and A. Rozza, "A robust approach for the background subtraction based on multi-layered self-organizing maps," *IEEE Transactions on Image Processing*, pp. 5239–5251, 2016.
- [65] Z. Zeng, J. Jia, D. Yu, Y. Chen, and Z. Zhu, "Pixel modeling using histograms based on fuzzy partitions for dynamic background subtraction," *IEEE Trans. Fuzzy Systems*, no. 3, pp. 584–593, June 2017.
- [66] S. Varadarajan, P. Miller, and H. Zhou, "Region-based mixture of gaussians modelling for foreground detection in dynamic scenes," *Pattern Recognit.*, no. 11, pp. 3488 – 3503, 2015.
- [67] A. Elgammal, D. Harwood, and L. Davis, "Non-parametric model for background subtraction," in *Eur. Conf. Comput. Vis. (ECCV)*, 2000, pp. 751–767.
- [68] B. Han, D. Comaniciu, and L. Davis, "Sequential kernel density approximation through mode propagation: Applications to background modeling," in *Asian Asian Conf. Comput. Vis. (ACCV)*, 2004.
- [69] Z. Liu, K. Huang, and T. Tan, "Foreground object detection using top-down information based on em framework," *IEEE Trans. Image Process.*, no. 9, pp. 4204–4217, Sept 2012.
- [70] D. Li, L. Xu, and E. Goodman, "A fast foreground object detection algorithm using kernel density estimation," in *IEEE Int. Conf. Signal Process.*, Oct 2012, pp. 703–707.
- [71] B. Gao, C. Xing, C. Xie, J. Wu, and X. Geng, "Deep label distribution learning with label ambiguity," *IEEE Transactions on Image Processing*, pp. 2825–2838, 2017.
- [72] Z. He, X. Li, Z. Zhang, F. Wu, X. Geng, Y. Zhang, M. Yang, and Y. Zhuang, "Data-dependent label distribution learning for age estimation," *IEEE Trans. on Image Process.*, 2017.
- [73] X. Geng, "Label distribution learning," *IEEE Trans. Knowledge and Data Engineering*, no. 7, pp. 1734–1748, July 2016.
- [74] P. Hou, X. Geng, Z.-W. Huo, and J. Lv, "Semi-supervised adaptive label distribution learning for facial age estimation," in *AAAI*, 2017.
- [75] X. Jia, W. Li, J. Liu, and Y. Zhang, "Label distribution learning by exploiting label correlations," 2018.
- [76] Z. Huo, X. Yang, C. Xing, Y. Zhou, P. Hou, J. Lv, and X. Geng, "Deep age distribution learning for apparent age estimation," in *Proceedings of the IEEE Conference on Computer Vision and Pattern Recognition (CVPR) Workshops*, June 2016.
- [77] C. Zhao, T. Cham, X. Ren, J. Cai, and H. Zhu, "Background subtraction based on deep pixel distribution learning," in *IEEE Int. Conf. Multimedia and Expo (ICME)*, July 2018.
- [78] C. Zhao and A. Basu, "Dynamic deep pixel distribution learning for background subtraction," *IEEE Transactions on Circuits and Systems for Video Technology*, vol. 30, no. 11, pp. 4192–4206, 2020.
- [79] A. Paszke, S. Gross, F. Massa, A. Lerer, J. Bradbury, G. Chanan, T. Killeen, Z. Lin, N. Gimelshein, L. Antiga *et al.*, "Pytorch: An imperative style, high-performance deep learning library," in *Advances in neural information processing systems*, 2019, pp. 8026–8037.
- [80] Y. Wang, P. M. Jodoin, F. Porikli, J. Konrad, Y. Benezeth, and P. Ishwar, "Cdnet 2014: An expanded change detection benchmark dataset," in *IEEE Conf. Comput. Vis. Pattern Recognit. Workshops (CVPRW)*, June 2014, pp. 393–400.
- [81] C. Cuevas, E. M. Yáñez, and N. García, "Labeled dataset for integral evaluation of moving object detection algorithms: Lasiesta," *Computer Vision and Image Understanding*, pp. 103 – 117, 2016.
- [82] D. Berjón, C. Cuevas, F. Morán, and N. García, "Real-time nonparametric background subtraction with tracking-based foreground update," *Pattern Recognit.*, pp. 156 – 170, 2018.
- [83] C. Cuevas and N. García, "Improved background modeling for real-time spatio-temporal non-parametric moving object detection strategies," *Image and Vision Computing*, no. 9, pp. 616 – 630, 2013.
- [84] H. Sajid and S. C. S. Cheung, "Universal multimode background subtraction," *IEEE Trans. Image Process.*, no. 7, pp. 3249–3260, July 2017.
- [85] P. L. St-Charles, G. A. Bilodeau, and R. Bergevin, "Universal background subtraction using word consensus models," *IEEE Trans. Image Process.*, no. 10, pp. 4768–4781, Oct 2016.
- [86] S. M. Roy and A. Ghosh, "Foreground segmentation using adaptive 3 phase background model," *IEEE Transactions on Intelligent Transportation Systems*, pp. 2287–2296, 2020.
- [87] L. Li, Q. Hu, and X. Li, "Moving object detection in video via hierarchical modeling and alternating optimization," *IEEE Transactions on Image Processing*, pp. 2021–2036, 2019.
- [88] S. E. Ebadi and E. Izquierdo, "Foreground segmentation with tree-structured sparse rpca," *IEEE Trans. Pattern Anal. Mach. Intell.*, Sep. 2018.
- [89] V. M. Mondéjar-Guerra, J. Rouco, J. Novo, and M. Ortega, "An end-to-end deep learning approach for simultaneous background modeling and subtraction," in *BMVC*, 2019.
- [90] O. Tezcan, P. Ishwar, and J. Konrad, "Bsuv-net: A fully-convolutional neural network for background subtraction of unseen videos," in *WACV*, March 2020.
- [91] A. Krizhevsky, I. Sutskever, and G. E. Hinton, "Imagenet classification with deep convolutional neural networks," *Advances in neural information processing systems*, vol. 25, pp. 1097–1105, 2012.
- [92] K. H. Y. Lim, Long Ang, "Learning multi-scale features for foreground segmentation," *arXiv*, 2018.
- [93] M. ul Hassan, "Vgg16 convolutional network for classification and detection," *Neurohive. Dostopno 2019*, 2018.
- [94] K. He, G. Gkioxari, P. Dollár, and R. Girshick, "Mask r-cnn," in *Proceedings of the IEEE International Conference on Computer Vision (ICCV)*, Oct 2017.
- [95] L. Chen, G. Papandreou, I. Kokkinos, K. Murphy, and A. L. Yuille, "Deeplab: Semantic image segmentation with deep convolutional nets, atrous convolution, and fully connected crfs," *IEEE Transactions on Pattern Analysis and Machine Intelligence*, vol. 40, no. 4, pp. 834–848, 2018.
- [96] J. Deng, W. Dong, R. Socher, L.-J. Li, K. Li, and L. Fei-Fei, "Imagenet: A large-scale hierarchical image database," in *CVPR*, 2009.
- [97] H. Zhang, C. Wu, Z. Zhang, Y. Zhu, Z. Zhang, H. Lin, Y. Sun, T. He, J. Mueller, R. Manmatha *et al.*, "Resnest: Split-attention networks," *arXiv preprint arXiv:2004.08955*, 2020.
- [98] L.-C. Chen, G. Papandreou, F. Schroff, and H. Adam, "Rethinking atrous convolution for semantic image segmentation," *arXiv preprint arXiv:1706.05587*, 2017.
- [99] D. P. Kingma and J. Ba, "Adam: A method for stochastic optimization," *arXiv preprint arXiv:1412.6980*, 2014.